Nuclear Physics B79 (1974) 10–37. North-Holland Publishing Company

# PHOTOPRODUCTION OF $\rho^0$, $\omega$ AND $\rho^-$ MESONS ON DEUTERONS AT ENERGIES BETWEEN 1 AND 5 GeV

P. BENZ *, O. BRAUN **, H. BUTENSCHÖN *, D. GALL *, U. IDSCHOK ***
C. KIESLING ‡, G. KNIES *, K. MÜLLER ***, B. NELLEN ***,
R. SCHIFFER ‡‡, P. SCHLAMP ‡, H.J. SCHNACKERS **, P. SÖDING *,
J. STIEWE ** and F. STORIM *
*Aachen – Bonn – Hamburg – Heidelberg – München Collaboration*

Received 1 April 1974
(Revised 6 May 1974)

Abstract: The reactions $\gamma d \to \rho^0 d$, $\gamma d \to \omega d$ and $\gamma n \to \rho^- p$ have been investigated in a deuterium bubble chamber experiment at DESY with a bremsstrahlung beam of 5.5 GeV maximum energy. Effective mass distributions as well as total and differential cross sections are presented. The results are compared with $\rho^0$ and $\omega$ production on protons.

## 1. Introduction

Photoproduction of neutral vector mesons is known to be a strongly diffractive process. The quantum numbers of the incoming and outgoing particles are identical, as in elastic scattering. Well established properties of diffractive vector meson production are the approximate independence of the amplitude on energy associated with a small real part, the predominant exchange of natural parity, and the nearly complete conservation of the boson's $s$-channel helicity.

The isospin properties of vector meson photoproduction are less well known. For a study of these properties experiments with neutron or deuteron targets are necessary. In most of the vector photoproduction experiments on deuterium carried out so far the sum of the coherent and break-up cross sections was measured [1]. Since the break-up process is difficult to analyze, interpretation of the results usually involves an extrapolation to $|t|_{\min}$ where the incoherent part becomes small. Indications were obtained for a non-negligible $I = 1$ exchange contribution to $\rho^0$ photoproduction on nucleons at $t \approx 0$ for photon energies of about 5 GeV [1].

* DESY und II. Institut für Experimentalphysik der Universität Hamburg.
** Institut für Hochenergiephysik der Universität Heidelberg.
*** Physikalisches Institut der Universität Bonn.
‡ Max-Planck-Institut für Physik und Astrophysik München.
‡‡ III. Physikalisches Institut, Lehrstuhl B der technischen Hochschule Aachen.

An experimentally cleaner way to investigate the isospin properties is to measure the coherent production

$$\gamma d \to \rho^0 d \tag{1}$$

separately, by detecting the final state deuteron. This was done in a counter experiment at SLAC where coherent $\rho^0$ production was measured in the double scattering region at large $|t|$; hence the contribution from elastic $\rho^0 N$ scattering could be investigated [2]. At smaller $|t|$ in the single scattering diffractive region reaction (1) has been measured by this group at DESY [3] and by a Weizmann group [4]; these were low statistics bubble chamber experiments. In the present paper, we present results with improved statistics in the energy region $0.9 < E_\gamma < 5.3$ GeV for $|t| < 0.2$ GeV$^2$. In the same experiment we have also observed coherent $\omega$ photoproduction

$$\gamma d \to \omega d. \tag{2}$$

In $\rho$ photoproduction, $I = 1$ exchange can also be studied in pure form in the charge exchange reaction

$$\gamma n \to \rho^- p. \tag{3}$$

Unfortunately, it is a difficult reaction to measure. We have published some cross sections previously [5] which were obtained from half of the statistics, and are now presenting our final results.

In sect. 2 of this paper we describe the event identification and the experimental corrections. The effective mass distributions and cross sections for the reactions (1), (2) and (3) are presented in sect. 3. The discussion of the results follows in sect. 4 with a determination of the coupling constant ratio $g^2_{\gamma\omega}/g^2_{\gamma\rho}$, an analysis of the isospin structure of the $\rho^0$ and $\omega$ photoproduction amplitude on nucleons and a test of Harari-Freund duality and Regge factorization.

## 2. Experimental procedure and identification of final states

The experiment was performed in the 85 cm deuterium bubble chamber at DESY, exposed to a bremsstrahlung beam of 5.5 GeV maximum energy. About 3.1 million pictures were taken. Details about the beam, the determination of the photon spectrum, and the scanning and measuring of the pictures have been described elsewhere [3, 6, 7]. A total of 85 000 photoproduction events were analyzed. For the kinematic analysis the program GRIND was used [8]. A description of the fitting procedure and a list of the reaction hypotheses considered were given in a previous publication [7].

### 2.1. The reaction $\gamma d \to \pi^+\pi^- d$

To identify the events belonging to the reaction

$$\gamma d \to \pi^+\pi^- d \tag{4}$$

the following criteria were applied:

(i) There had to be a three constraint (3c) kinematic fit to reaction (4) with a $\chi^2$ probability $P(\chi^2) > 0.1$ %.

(ii) The agreement between the calculated and observed ionization of all tracks had to be satisfactory, and range-energy constraints had to be fulfilled.

(iii) The momentum $|\boldsymbol{p}_d|$ of the final state deuteron in the lab system had to be $|\boldsymbol{p}_d| < 0.45$ GeV/$c$, corresponding to $t = (p_\gamma - p_{\pi^+\pi^-})^2 > -0.2$ GeV$^2$. This was required because on part of the pictures only events with $|\boldsymbol{p}_d| \lesssim 0.56$ GeV/$c$ had been measured.

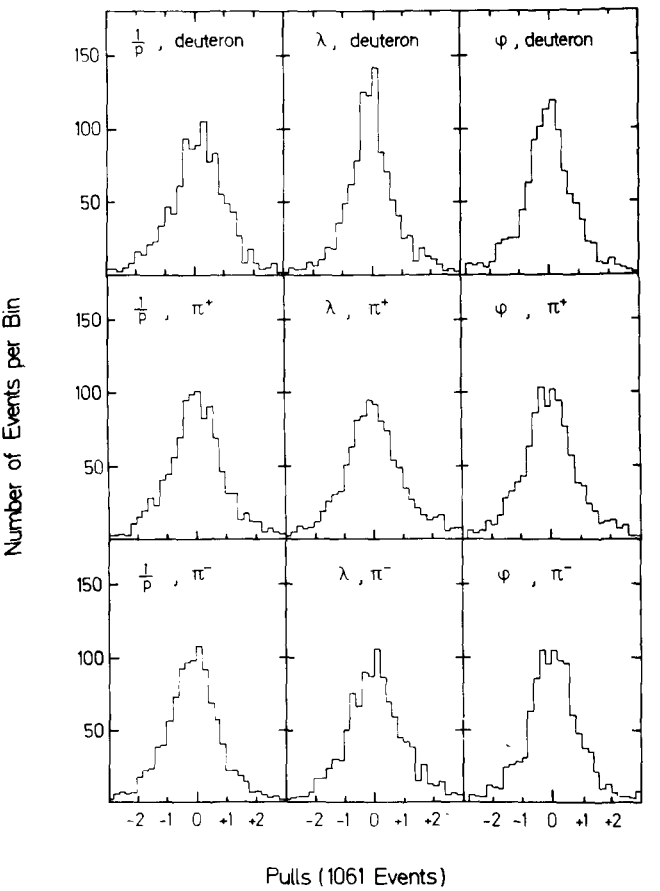


Fig. 1. Pulls for three-prong events of the reaction $\gamma d \to \pi^+\pi^- d$. $p$ is the momentum, $\lambda$ the dip angle and $\varphi$ the azimuthal angle of the track with respect to the optical axis. The pull is defined as the difference between the measured and the fitted value, divided by the error of this difference.

We found 3 551 events satisfying these criteria. Among these events, 45 % had only two prongs, since the deuteron track was invisible; the deuteron lab momentum is then $|\boldsymbol{p}_d| \lesssim 0.165$ GeV/$c$. Studies with Monte-Carlo simulated events showed that a reliable distinction between reaction (4) and the deuteron break-up reaction

$$\gamma d \to \pi^+ \pi^- \text{ pn} \tag{5}$$

is not possible for two-prong events [3]. Therefore we had to restrict ourselves to the three-prong events (which have a visible deuteron track). For further analysis we only used the three-prong events in the $t$-range $0.04 < |t| < 0.20$ GeV$^2$, since the fraction of two-prong events in this kinematic range is small and can be corrected for (see below). We found 1061 of these events in the photon energy range $0.9 < E_\gamma < 5.3$ GeV.

As a check for possible biases in the kinematic fits we have investigated the pulls [7]. As is seen in fig. 1, they are symmetrically distributed around zero.

To check the event identification we generated Monte-Carlo events of reaction (4) and of other reactions, and subjected them to our selection procedure as described above. For the Monte-Carlo events the identification of reaction (4) was found to be free from bias within better than 1%. For true events, however, the situation may be worse due to various effects unknown in detail, which may not have been properly simulated in the Monte-Carlo calculations. Thus, for example, true events from reaction (4) may fail the 3c-fit due to an unnoticed scatter of the deuteron near the event vertex. Most of the events which fail the 3c-fit will fall into the sample assigned to reaction (5) for which only a 0c-fit is required. (For some of these events the reaction hypothesis $\gamma d \to \pi^0 \pi^+ \pi^- d$ is also possible, but nearly all ($> 98$ %) of the events that fit the latter reaction also fit reaction (5).) In the spurious 0c-fits to reaction (5), the angle between the momenta of the reconstructed neutron and the proton is always small, corresponding to a small proton-neutron effective mass. Furthermore, these fits will always have a spurious proton momentum $|\boldsymbol{p}_p|$ greater than the calculated neutron momentum $|\boldsymbol{p}_n|$, since momentum balance requires $\boldsymbol{p}_p + \boldsymbol{p}_n = \boldsymbol{p}_d$ whereas for a stopping deuteron $\boldsymbol{p}_p \approx 0.6\, \boldsymbol{p}_d$ from the range and for a leaving deuteron $\boldsymbol{p}_d \approx \boldsymbol{p}_d$ from curvature. Indeed there is an indication of an excess at 0° in the distribution of the lab break-up angle between the proton and the neutron, for the events that fit reaction (5) but not reaction (4) and that have $|\boldsymbol{p}_p| > |\boldsymbol{p}_n|$; no such irregularity is observed for events with $|\boldsymbol{p}_p| < |\boldsymbol{p}_n|$ (see fig. 2). From this excess the fraction of the events of reaction (4) that fail the kinematic fit and turn up in the event sample of reaction (5) could be estimated. It leads to a correction that depends on $t$ and reaches + 10% at large $|t|$.

There are also events of reaction (4) that fail the kinematic fits to both reactions (4) and (5). In that case they cannot be fitted by any hypothesis at all. These losses add to the losses of events which were unmeasurable for various reasons and necessitate an overall correction of (+5 ± 2)%. The correction for losses of events at the scanning stage is (+5 ± 3)%.

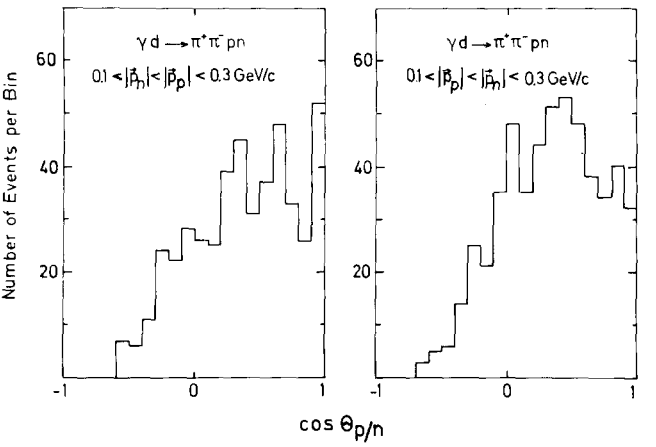


Fig. 2. Distribution of the lab break-up angle between the proton and the neutron for three-prong events of the reaction $\gamma d \to \pi^+\pi^-pn$, which are not ambiguous with the reaction $\gamma d \to \pi^+\pi^-d$.

Finally, since we use only three-prong events in the analysis a further correction has to be made for three-prong events being mistaken as two-prong events. This can occur when the deuteron track is overlapping in the film plane with one of the outgoing pion tracks. Azimuthal symmetry of the tracks around the beam direction was used [9] to correct for this effect, which particularly affects the events at small $|t|$ (up to about +10%).

In summary we have obtained 1061 three-prong events of reaction (4) in the kinematic region $0.9 < E_\gamma < 5.3$ GeV and $0.04 < |t| < 0.20$ GeV$^2$. This sample is free of contamination but has to be corrected for various types of inefficiencies. The correction depends on $t$ (+ 20% on the average). All cross sections presented below are given a systematic error of ± 7% which includes the uncertainties of the experimental corrections as well as those of the shape and normalization of the photon energy spectrum.

### *2.2. The reaction $\gamma d \to \omega d$*

To investigate coherent $\omega$ production on the deuteron we have to study the reaction

$$\gamma d \to \pi^0\pi^+\pi^- d. \tag{6}$$

Since this reaction allows only a kinematic 0c-fit, it cannot be separated from other 0c-fit reactions like, e.g., reaction (5). Fortunately the $\omega$ is a rather narrow resonance which stands out clearly above the background. Therefore, we can separate the $\omega$ from the background directly in the effective $\pi^0\pi^+\pi^-$ mass distribution of all events which are compatible with reaction (6) according to kinematics and ionization of the

tracks. There were 865 such events with three visible tracks in the kinematic range $1.4 < E_\gamma < 5.3$ GeV and $0.05 < |t| < 0.20$ GeV$^2$. The corrections for scanning losses of three-prong events and for losses of unmeasurable events are the same as for reaction (4).

### 2.3. The reaction $\gamma d \to \pi^0 \pi^- pp$

Finally we discuss the selection of events belonging to the reaction

$$\gamma d \to \pi^0 \pi^- pp. \tag{7}$$

A kinematic discrimination between reaction (7) and the reaction $\gamma d \to \pi^- pp$ is possible and has been discussed in detail in a previous paper [7]. However, kinematic ambiguities of the 0c-fit to reaction (7) exist with the reactions $\gamma d \to \pi^+ \pi^- d$, $\gamma d \to \pi^0 \pi^+ \pi^- d$, $\gamma d \to \pi^+ \pi^- pn$ and $\gamma d \to \pi^0 \pi^- pp + m\pi^0$ ($m \geqslant 1$). The ambiguity with the first three reactions is due to insufficient $\pi^+$/p/d discrimination at high lab momenta; it can be avoided by a restriction to small $-t = -(p_\gamma - p_{\pi^0\pi^-})^2$. For the study of $\rho^-$ production we therefore used only events in the kinematic region $|t| < 1.1$ GeV$^2$.

On the other hand, a separation of the single $\pi^0$ reaction (7) from multiple $\pi^0$ events is not possible by kinematics or ionization. (Note that the photon energy was not measured, but had to be calculated from energy and momentum conservation.) Therefore we always have to take this background into account when we try to extract $\rho^-$ cross sections. This will be further discussed in subsect. 3.3.

The corrections applied to the data include corrections for scanning losses (+ 5%), events with no acceptable hypotheses (+4%), and events that give spurious fits to the reaction $\gamma d \to \pi^- pp$ (+4%). Furthermore, the effect of the finite photon energy resolution was unfolded from the photon energy dependence of the cross sections. These finite resolution effects are due to measuring errors and to systematic shifts of the calculated kinematical quantities in case of two-prong events, where the momentum of the invisible proton was fixed at zero in the kinematic fit. The systematic uncertainties of these corrections as well as those of the shape and normalization of the photon energy spectrum sum up to ± 12 %, which are included in the error bars of all cross sections given below.

The extraction of information from reaction (7) on the reaction

$$\gamma n \to \pi^0 \pi^- p \tag{8}$$

by means of the spectator model will be discussed in subsect. 3.3.1.

## 3. Experimental results

### 3.1. The reaction $\gamma d \to \rho^0 d$

*3.1.1. Cross section for the reaction $\gamma d \to \pi^+ \pi^- d$.* The cross section of the reaction (4), $\gamma d \to \pi^+ \pi^- d$, is shown in fig. 4a as a function of the lab photon energy $E_\gamma$

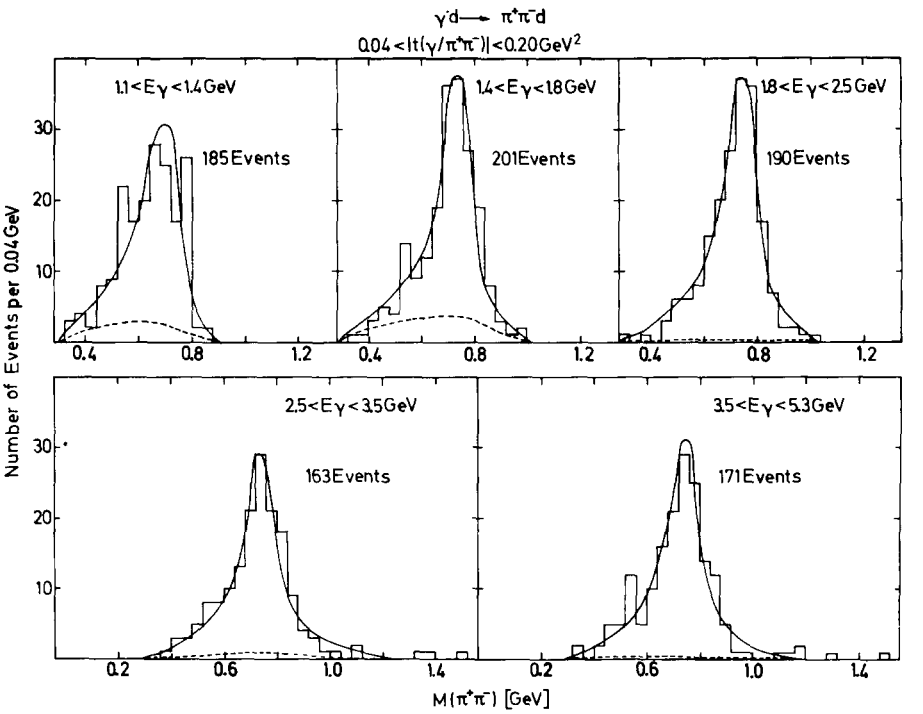
γd→ π⁺π⁻d
0.04<|t(γ/π⁺π⁻)|<0.20GeV²
1.1<Eγ<1.4GeV
185Events
1.4<Eγ<1.8GeV
201Events
1.8<Eγ<2.5GeV
190Events
2.5<Eγ<3.5GeV
163Events
3.5<Eγ<5.3GeV
171Events
Number of Events per 0.04GeV
M(π⁺π⁻) [GeV]

Fig. 3a.

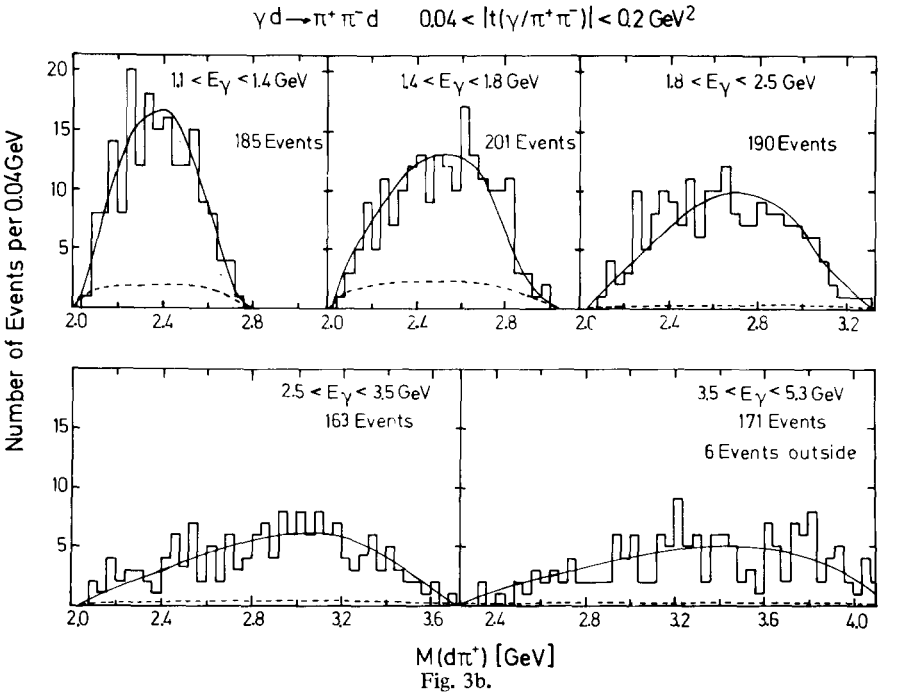
γ d→π⁺ π⁻ d 0.04 < |t(γ/π⁺π⁻)| < 0.2 GeV²
1.1 < Eγ < 1.4 GeV
185 Events
1.4 < Eγ < 1.8 GeV
201 Events
1.8 < Eγ < 2.5 GeV
190 Events
2.5 < Eγ < 3.5 GeV
163 Events
3.5 < Eγ < 5.3 GeV
171 Events
6 Events outside
Number of Events per 0.04GeV
M(dπ⁺) [GeV]

Fig. 3b.

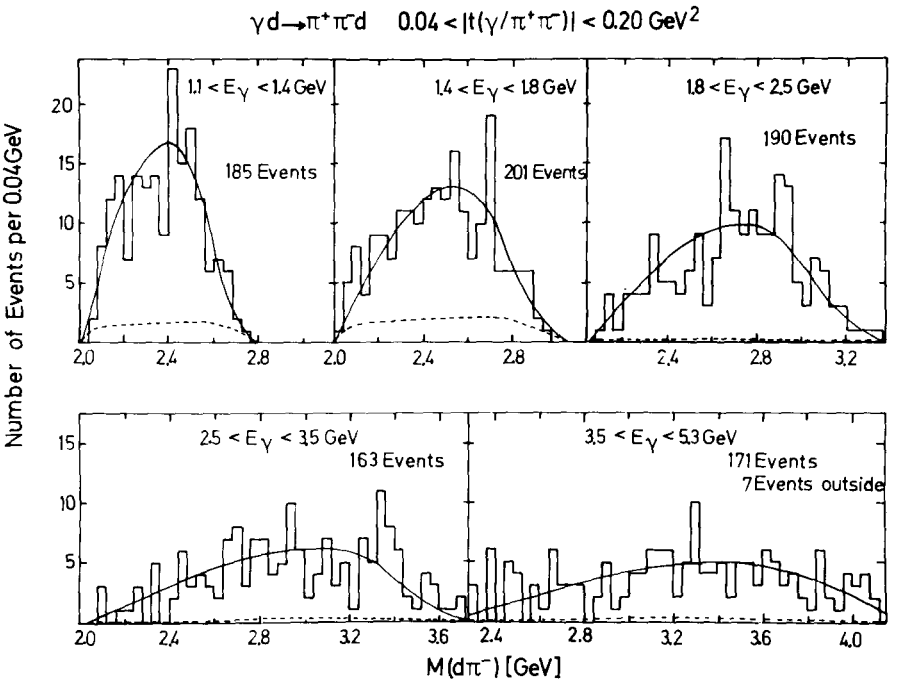


Fig. 3c.

Fig. 3. (a–c) Effective mass distributions of the $\pi^+\pi^-$, $\pi^+$d and $\pi^-$d systems in the reaction $\gamma d \to \pi^+\pi^- d$ for the $t$-range $0.04 < |t| < 0.20$ GeV$^2$ and various intervals of $E_\gamma$. The full (dashed) curves show the total (background) distribution obtained by fits using assumption (i) on the resonance shape (see subsect. 3.1.2).

between 0.9 and 5.3 GeV. For the reasons discussed in subsect. 2.1, the $t$-range is restricted to $0.04 < |t| < 0.20$ GeV$^2$ where $t = (p_\gamma - p_{\pi^+\pi^-})^2$.

*3.1.2. $\rho^0$ production.* The effective mass distributions of the $\pi^+\pi^-$, $\pi^+$ d and $\pi^-$d systems in reaction (4) are shown in figs. 3a–c for various intervals of $E_\gamma$. The production of the $\rho^0$ is the only apparent resonance production process. In fact there is very little background underneath the $\rho^0$ resonance for $E_\gamma > 1.8$ GeV. For $E_\gamma <$ 1.4 GeV, on the other hand, it is not easy to determine how much $\rho^0$ is present due to the kinematic limitations on $t$ and $M_{\pi^+\pi^-}$. (Note that the minimum photon energy required to produce a $\rho^0$ of resonance mass at $|t| = 0.04$ GeV$^2$ on deuterons is $E_\gamma = 1.64$ GeV.) Hence the amount of $\rho^0$ deduced is strongly dependent on the mass shapes assumed for the resonance and the background. The $\pi^+$d and $\pi^-$d mass distributions are well described by $\rho^0$ reflection plus phase space background, as we will show below.

The cross section for coherent $\rho^0$ production (reaction (1)) has been determined by fits to the data shown in fig. 3. Three different assumptions on the resonance shape were used:

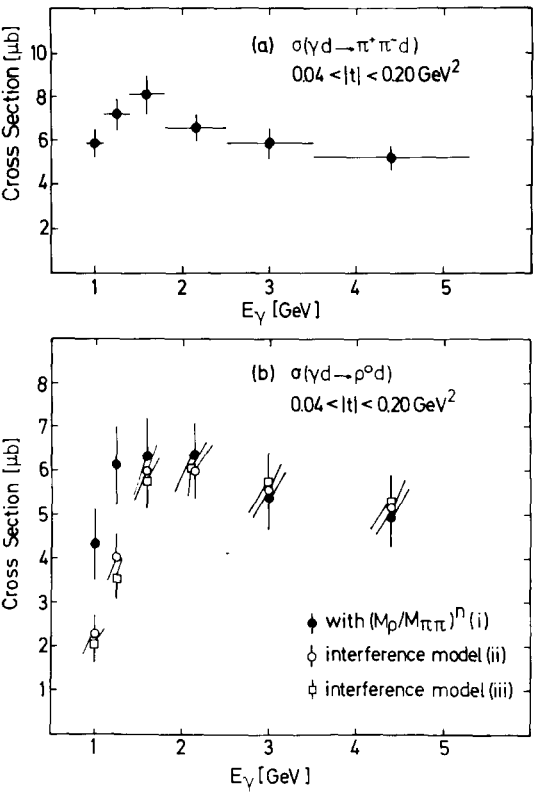


Fig. 4 (a) Cross sections of the reaction $\gamma d \to \pi^+\pi^- d$ as a function of $E_\gamma$ for the $t$-range $0.04 < |t| < 0.2$ GeV$^2$. (b) Cross section of the reaction $\gamma d \to \rho^0 d$ as a function of $E_\gamma$ for the $t$-range $0.04 < |t| < 0.2$ GeV$^2$. The values are obtained by fits using assumption (i) (black dots), (ii) (open circles) and (iii) (open squares) on the resonance shape (see subsect. 3.1.2).

(i) In the first fit, we used a $\rho^0$ Breit-Wigner enhancement

$$\frac{M_{\pi\pi}}{\pi^2 q(M_{\pi\pi})}\,\frac{M_\rho \Gamma(M_{\pi\pi})}{(M_\rho^2 - M_{\pi\pi}^2)^2 + M_\rho^2\,\Gamma^2(M_{\pi\pi})}, \tag{9}$$

$$\Gamma(M_{\pi\pi}) = \Gamma_\rho \left[\frac{q(M_{\pi\pi})}{q(M_\rho)}\right]^3 \frac{2q^2(M_\rho)}{q^2(M_{\pi\pi}) + q^2(M_\rho)}, \qquad q^2(M_{\pi\pi}) = \tfrac{1}{4} M_{\pi\pi}^2 - m_\pi^2,$$

multiplied by a factor [10] $(M_\rho/M_{\pi\pi})^{n(t)}$; this was added incoherently to a phase space background term. Both resonance and background terms were multiplied by a factor exp (24 $t$) to describe the experimental $t$ distribution (see below). Besides the amounts of resonance and background, also the parameters $M_\rho$, $\Gamma_\rho$ and n were fitted. From all the fits to the data for $E_\gamma > 1.4$ GeV we found $M_\rho = 0.762 \pm 0.005$ GeV, $\Gamma_\rho = 0.152 \pm 0.005$ GeV and $n(t) = (5.6 \pm 0.5) + (14.9 \pm 5.8)$ GeV$^{-2} \cdot t$. The curves shown in fig. 3 are obtained from these fits.

(ii) Another assumption was to have a diffractive resonance amplitude $T_\rho$ interfering with the Drell one-pion exchange terms $T_D$ [11–13]. The $\pi^\pm$d elastic scattering amplitudes entering in the Drell terms were calculated from the $\pi^\pm$p elastic scattering amplitudes in the impulse approximation [14]. The complete amplitude is

$$T_\rho + T_D \exp(i\delta) \cos\delta, \tag{10}$$

where $\delta$ is the elastic $\pi^+\pi^-$ scattering phase shift. The factor $\exp(i\delta)\cos\delta$ modifies the Drell terms such as to avoid double counting of $\rho^0$ resonance production [15–17]. Since the Drell terms can be calculated, only the resonance amplitude $T_\rho$ was fitted.

(iii) The factor $\exp(i\delta)\cos\delta$ causes the non-resonant term in (10) to vary relatively rapidly in the neighbourhood of the $\rho^0$, in contrast with the behaviour generally associated with a non-resonant background amplitude. One may therefore redefine the resonant part of the amplitude by splitting the complete amplitude (10) into a slowly and a rapidly varying part [18],

$$T_\rho + T_D \exp(i\delta)\cos\delta \equiv T_\rho + T_D (1 + i \exp(i\delta)\sin\delta)$$

$$\equiv T_{res} + T_D,$$

with

$$T_{res} = T_\rho + i\, T_D \exp(i\delta)\sin\delta.$$

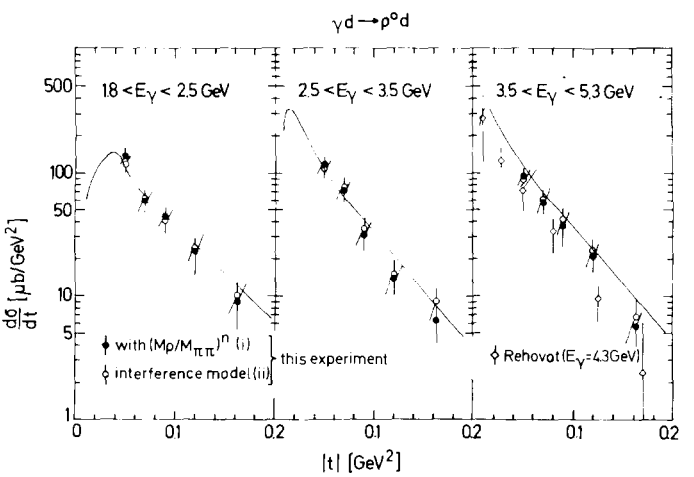


Fig. 5. Differential cross sections of the reaction $\gamma d \to \rho^0 d$. The values are obtained by fits using assumption (i) (black dots) and (ii) (open circles) on the resonance shape (see subsect. 3.1.2). Also shown are the results of the Weizmann group [4] (diamonds) at $E_\gamma$ = 4.3 GeV. The curves are predictions from the reaction $\gamma p \to \rho^0 p$ assuming equal $\rho^0$ photoproduction amplitudes on the proton and the neutron.

We will also give the $\rho^0$ cross sections obtained with this definition of the resonant part. In both cases (ii) and (iii), the values $M_\rho$ = 0.765 GeV and $\Gamma_\rho$ = 0.130 GeV were used.

*3.1.3. Total and differential cross sections for the reaction $\gamma d \to \rho^0 d$.* The cross sections $\sigma(\gamma d \to \rho^0 d)$ determined with each of these three different assumptions are shown in fig. 4b *. The different assumptions lead to nearly identical cross-section values, except in the region $E_\gamma < 1.4$ GeV where threshold effects make the analysis somewhat uncertain. After a steep rise above threshold, the cross section is energy-independent as expected for a purely diffractive production mechanism.

Differential $\rho^0$ production cross sections were determined from the data by repeating the above fits independently in various $t$-bins. The results for $E_\gamma > 1.8$ GeV are shown in fig. 5. The differential cross section values obtained with assumption (iii) do not differ from those obtained with assumption (ii) and therefore are not shown in fig. 5. The results of the Weizmann group [4] for $d\sigma/dt(\gamma d \to \rho^0 d)$ at $E_\gamma$ = 4.3 GeV are also shown in fig. 5 (diamonds). They seem to be systematically smaller than ours. We cannot explain this discrepancy but are confident that our normalization cannot be grossly wrong (cf. subsect. 2.1 and ref. [7]).

For comparison with differential cross sections of other processes like $\gamma d \to \omega d$ or $\gamma p \to \rho^0 p$, it is useful to correct for the kinematic turnover of $d\sigma/dt$ at small $|t|$

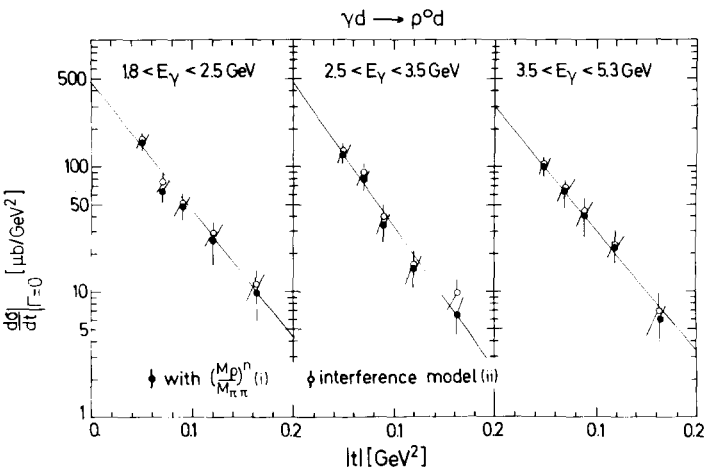


Fig. 6. Differential cross sections of the reaction $\gamma d \to \rho^0 d$ after correcting for the finite width of the $\rho^0$ (subsect. 3.1.3). The symbols are the same as defined in fig. 5. The lines are obtained from a fit of an exponential to the data (assumption (ii)).

* The cross section values of fig. 4b supersede the preliminary results from our earlier publication [3]. The final results presented here are obtained from better statistics, improved experimental corrections and a refined analysis of $\rho^0$ production.

(see fig. 5) which arises from the fact that for fixed $E_\gamma$ the kinematically possible maximum value of $M_{\pi^+\pi^-}$ depends on $t$, thus producing a variable cutoff in the mass distribution of a wide resonance like the $\rho$. We write for the observed resonance production differential cross section [19]

$$\left.\frac{d\sigma}{dt}\right|_{\text{finite }\Gamma} = \int_{4m_\pi^2}^{\max M_{\pi\pi}^2(t)} dM_{\pi\pi}^2 \, f_{\text{res}}(M_{\pi\pi}) \frac{d\sigma_0}{dt}(M_{\pi\pi}),$$

where

$$f_{\text{res}}(M_{\pi\pi}) = \frac{\sin^2 \delta(M_{\pi\pi})}{\pi M_{\text{res}} \Gamma(M_{\pi\pi})},$$

and $d\sigma_0/dt(M_{\pi\pi})$ is the cross section to produce the resonant $\pi\pi$ system in a state of mass $M_{\pi\pi}$. To first approximation $d\sigma_0/dt\,(M_{\pi\pi})$ does not vary over the width of the resonance and can therefore be replaced by $d\sigma/dt|_{\Gamma=0}$; thus

$$\left.\frac{d\sigma}{dt}\right|_{\text{finite }\Gamma} = \left.\frac{d\sigma}{dt}\right|_{\Gamma=0} \int_{4m_\pi^2}^{\max M_{\pi\pi}^2(t)} dM_{\pi\pi}^2 \, f_{\text{res}}(M_{\pi\pi}).$$

The $t$-dependent integral then gives the kinematic correction due to the finite width. Note that in calculating the total cross section

$$\sigma_{\Gamma=0} = \int_{|t|_{\min}}^{|t|_{\max}} \left.\frac{d\sigma}{dt}\right|_{\Gamma=0} dt \qquad (11)$$

Table 1
Results of fitting an exponential $A \exp(Bt)$ to the differential cross sections $d\sigma/dt|_{\Gamma=0}$ (corrected for finite width effects) for coherent $\rho^0$ production, $\gamma d \to \rho^0 d$, in the $t$-range $0.04 < |t| < 0.20$ GeV$^2$. (The model assumptions are explained in subsect. 3.1.2.)

| $E_\gamma$ (GeV) | 1.8 – 2.5 | 2.5 – 3.5 | 3.5 – 5.3 | 1.8 – 5.3 | model |
|---|---|---|---|---|---|
| $A$ ($\mu$b · GeV$^{-2}$) | 467 ± 144 | 541 ± 148 | 335 ± 77 | 410 ± 67 | assumption |
| $B$(GeV$^{-2}$) | 25.5 ± 3.9 | 29.5 ± 3.2 | 24.2 ± 2.5 | 25.5 ± 1,8 | (i) |
| $A$ ($\mu$b · GeV$^{-2}$) | 468 ± 108 | 470 ± 120 | 312 ± 75 | 383 ± 60 | assumption |
| $B$(GeV$^{-2}$) | 23.8 ± 2.7 | 26.5 ± 3.1 | 22.6 ± 2.8 | 23.7 ± 1.8 | (ii) |
| $A$ ($\mu$b · GeV$^{-2}$ | 481 ± 111 | 501 ± 129 | 327 ± 83 | 402 ± 65 | assumption |
| $B$(GeV$^{-2}$) | 24.0 ± 2.7 | 26.9 ± 3.2 | 22.9 ± 2.9 | 24.0 ± 1.8 | (iii) |

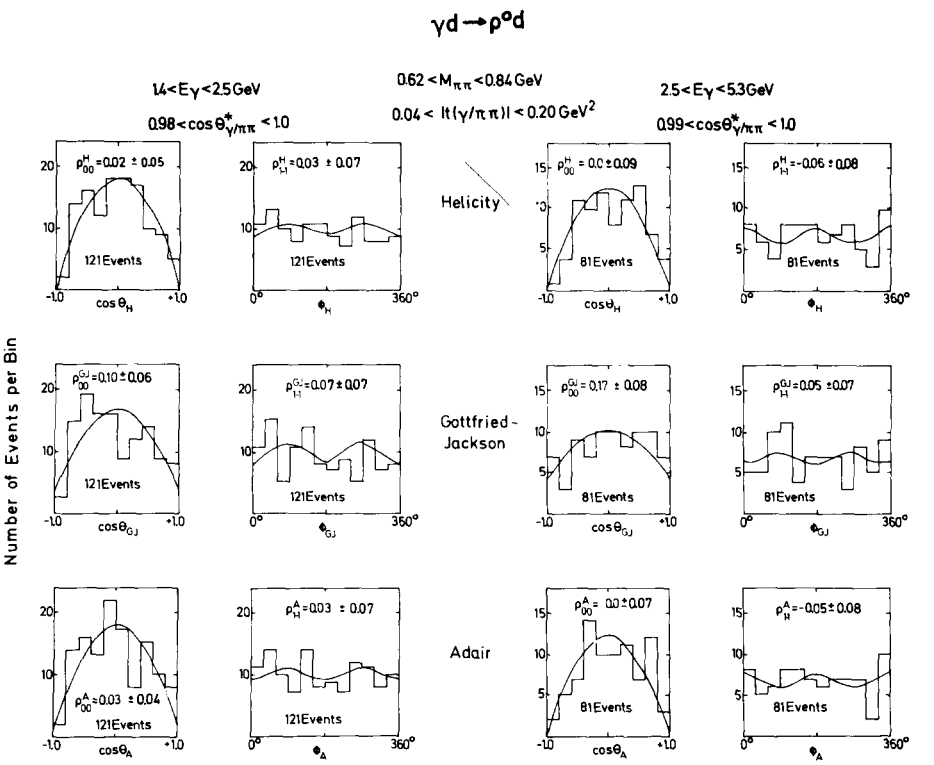


Fig. 7. Decay angular distributions of the $\pi^+\pi^-$ system for events of the reaction $\gamma d \to \pi^+\pi^- d$ with $M(\pi^+\pi^-)$ in the $\rho^0$ mass region and cms production angles of the $\pi^+\pi^-$ system near the forward direction. The coordinate systems are defined in subsect. 3.1.4. The curves are obtained from fits of the $\rho^0$ density matrix elements.

for resonance production, the limits of integration are those calculated for the resonance mass.

The corrected differential cross sections $d\sigma/dt|_{\Gamma=0}$ for the reaction (1) are shown in fig. 6. For the correction of the differential cross sections obtained with assumption (i), $f_{\text{res}}(M_{\pi\pi})$ was multiplied by a factor $(M_\rho/M_{\pi\pi})^4$. A fit of an exponential form

$$\left.\frac{d\sigma}{dt}\right|_{\Gamma=0} = A \exp(Bt)$$

to these differential cross sections gives values of A and B as shown in table 1. With the assumption that $d\sigma/dt$ is exponential throughout, the total cross section of reaction (1) corrected for the finite width effect can be calculated from eq. (11). The result obtained does not depend on the assumed $\rho^0$ resonance shape. As an average over the photon energy range $1.8 < E_\gamma < 5.3$ GeV we obtain $\sigma_{\Gamma=0}(\gamma d \to \rho^0 d) = 13 \pm 2\ \mu b$.

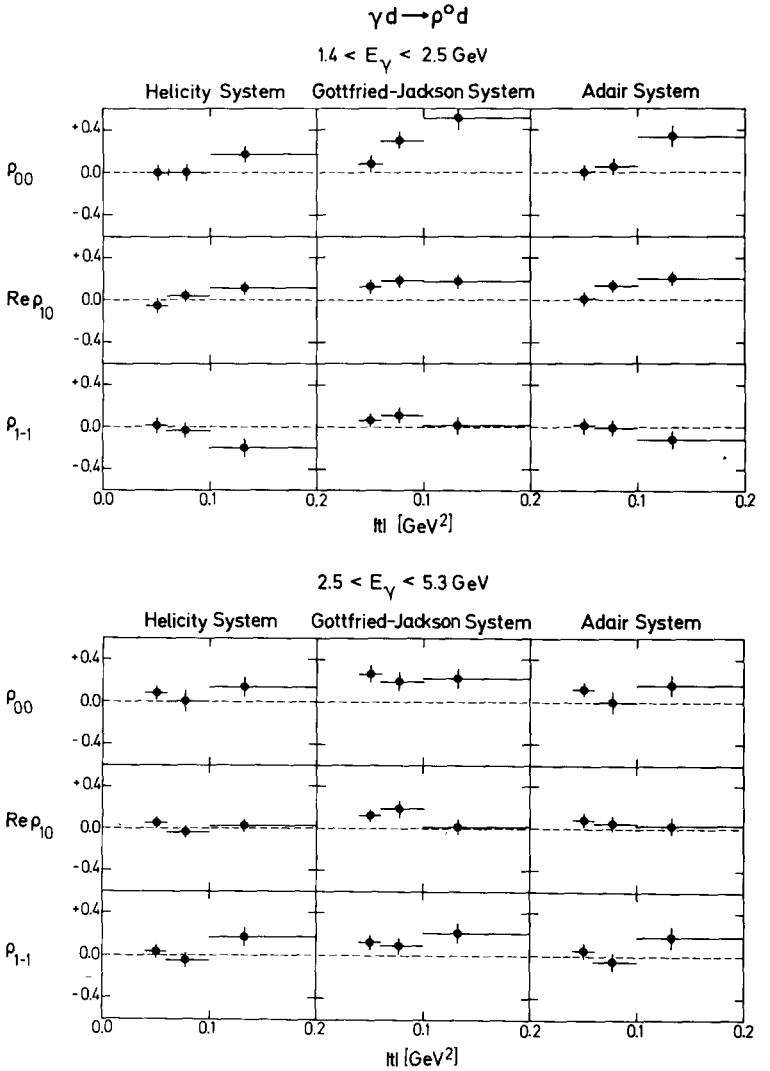


Fig. 8. $\rho^0$ density matrix elements as a function of $t$. The coordinate systems are defined in subsect. 3.1.4.

*3.1.4. $\rho^0$ decay.* The decay angular distributions of the $\pi^+\pi^-$ systems in the $\rho^0$ mass region and with cms production angles near the forward direction are shown in fig. 7. Three different choices of the quantization axis $\hat{z}$ are used. In the helicity system $\hat{z}$ is parallel to the cms momentum of the $\rho^0$, while in the Gottfried-Jackson and Adair systems $\hat{z}$ is parallel to the photon momentum in the $\rho^0$ rest frame or in the overall cms, respectively. From fits to these decay angular distributions the

curves and the density matrix elements given in fig. 7 were obtained. Fig. 8 shows the $t$-dependence of the density matrix elements $\rho_{00}$, Re $\rho_{10}$ and $\rho_{1-1}$. Near the forward direction the helicity density matrix element $\rho_{00}$ is compatible with zero, i.e. with $s$-channel helicity conservation.

### 3.2. The reaction $\gamma d \to \omega d$

In fig. 9 the effective mass distribution of the three-pion system of all three-prong events fitting hypothesis (6), $\gamma d \to \pi^0\pi^+\pi^- d$, is shown (unshaded histogram). The kinematic range is restricted to $1.4 < E_\gamma < 5.3$ GeV and $0.05 < |t| < 0.20$ GeV$^2$. No clear $\omega$ enhancement is seen in the large background. This background can be reduced by using only events in the central region of the three-pion Dalitz plot, since the density distribution for the decay of a $J^P = 1^-$ resonance into three pions has its maximum in the centre of the Dalitz plot [20]. A central region, con-

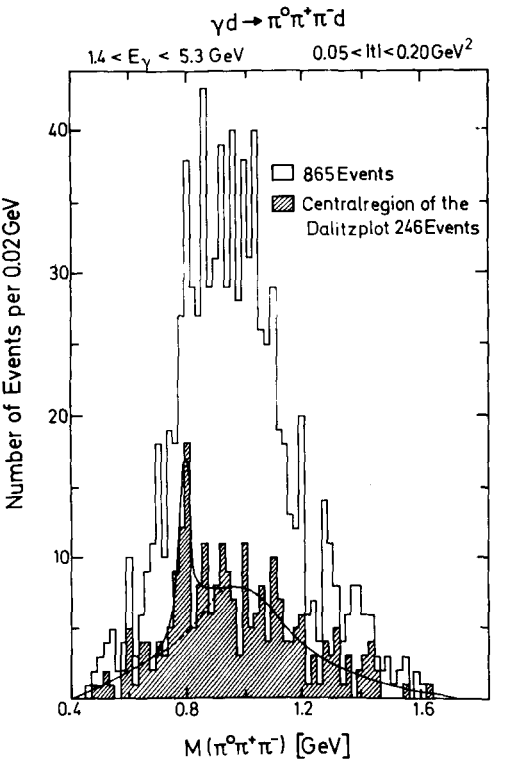


Fig. 9. Distribution of the effective $\pi^0\pi^+\pi^-$ mass for three-prong events of the reaction $\gamma d \to \pi^0\pi^+\pi^- d$ in the kinematic region $1.4 < E_\gamma < 5.3$ GeV and $0.05 < |t| < 0.20$ GeV$^2$ (unshaded histogram). The distribution of the events in the central region of the Dalitz plot (see subsect. 3.2) is shown by the shaded histogram. The curve is obtained by a fit of $\omega$ and background contributions.

taining exactly 50 % of all true $\omega \to \pi^+\pi^-\pi^0$ decays, can be defined in a mass independent way by

$$\frac{|\boldsymbol{p}_+ \times \boldsymbol{p}_-|^2}{(M^2(\pi^0\pi^+\pi^-) - 9m_\pi^2)^2} > 0.0065,$$

where $\boldsymbol{p}_+$ and $\boldsymbol{p}_-$ are the momenta of the $\pi^+$ and $\pi^-$ in the three-pion rest system [21]. The shaded histogram in fig. 9 shows the $M(\pi^0\pi^+\pi^-)$ distribution for this central region. A clear $\omega$ signal is now observed.

The fraction of $\omega$ production was determined by fitting to the shaded histogram of fig. 9 an incoherent superposition of a hand-drawn background with two free parameters, and a non-relativistic Breit-Wigner folded with a mass resolution function of triangular shape [22] (full curve in fig. 9). The resonance parameters were fixed. The cross section thus obtained is $\sigma(\gamma d \to \omega d) = (0.64\ ^{+0.17}_{-0.31})\ \mu b$ for $1.4 < E_\gamma < 5.3$ GeV and $0.05 < |t| < 0.20$ GeV$^2$. This number is corrected for the unobserved $\omega\pi$ decay modes, and the negative error has been enlarged in view of the difficulty of estimating the shape of the background.

### *3.3. The reaction $\gamma n \to \rho^- p$*

We now discuss the reactions (8), $\gamma n \to \pi^0\pi^- p$, and (3), $\gamma n \to \rho^- p$ [23, 24], which are deduced from the reaction (7), $\gamma d \to \pi^0\pi^- pp_s$, by means of the spectator mo-

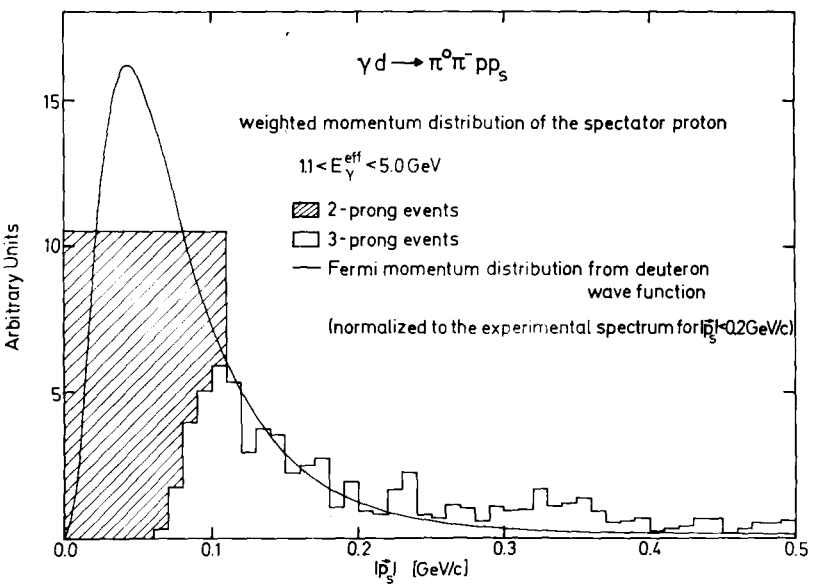


Fig. 10. Lab. momentum distribution of the lower-energy proton in the reaction $\gamma d \to \pi^0\pi^- pp$. Each event is weighted such as to unfold phase space and photon spectrum effects [7]. The solid curve is the Fermi momentum distribution calculated from the deuteron wave function [25, 26] and normalized to the observed number of weighted events with $|p_s| < 0.2$ GeV/$c$.

del. As appropriate energy variable we use the effective lab photon energy

$$E_\gamma^{\text{eff}} = (s - m_n^2)/2m_n, \tag{12}$$

where $s$ is the square of the invariant mass of the $\pi^0\pi^-$p system and $m_n$ the on-shell neutron's mass. $E_\gamma^{\text{eff}}$ is the photon energy required to give the c.m.s. energy $\sqrt{s}$ with an on-shell target neutron at rest.

*3.3.1. Provisions for the use of the spectator model.* In order to determine cross sections on the neutron as target particle from our data, we have tried to select a subsample of events in which one of the protons can be approximately considered to be a spectator. We show in fig. 10 the distribution of the momentum $|\boldsymbol{p}_s|$ of the slower one of the two protons in reaction (7). The shaded area corresponds to the amount of invisible proton tracks ($|\boldsymbol{p}_s| \lesssim 0.1$ GeV/$c$). The events are weighted such as to unfold phase space and photon spectrum effects [7]. If all of the lower-energy protons were spectators, the distribution should agree with the Fermi momentum distribution in the deuteron which is shown for comparison, normalized to the observed number of events in the range $0 < |\boldsymbol{p}_s| < 0.2$ GeV/$c$. It has been calculated from a modified Hamada-Johnston wave function [25] in the parametrization of J. Humberston which is quoted in ref. [26]. Approximate agreement between the data and the theoretical distribution is observed for $|\boldsymbol{p}_s| < 0.2$ GeV/$c$, but clear deviations occur at higher $|\boldsymbol{p}_s|$.

To check further whether protons with $|\boldsymbol{p}_s| < 0.2$ GeV/$c$ can be considered to be spectators to sufficient accuracy, we study the distribution of the Treiman-Yang angle $\varphi_T$ for these protons [27, 28]. This angle is defined as the azimuthal angle of $\boldsymbol{p}_s$ in the rest frame of the photon and the exchanged neutron, i.e.

$$\cos\varphi_T = \frac{\boldsymbol{p}_d \times \boldsymbol{p}_s}{|\boldsymbol{p}_d \times \boldsymbol{p}_s|} \cdot \frac{\boldsymbol{p}_{\pi^0} \times \boldsymbol{p}_\gamma}{|\boldsymbol{p}_{\pi^0} \times \boldsymbol{p}_\gamma|}.$$

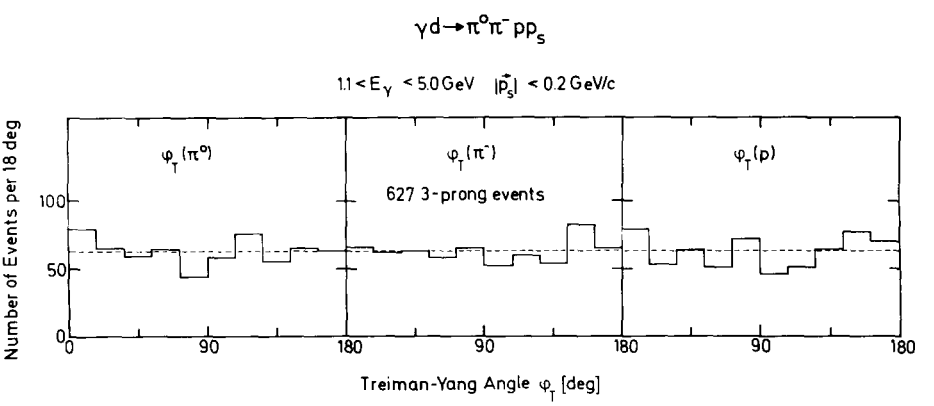


Fig. 11. Treiman-Yang angular distributions for the $\pi^0$, $\pi^-$ and the higher-energy proton in the reaction $\gamma d \to \pi^0\pi^-pp$.

Instead of $\boldsymbol{p}_{\pi 0}$, also the momentum vector of the $\pi^-$ or of the faster proton can be used to define the plane $\varphi_T = 0$. In all cases these distributions must be flat if a single neutron is exchanged as the spectator picture assumes. This can be checked for three-prong events (i.e. events with a visible spectator) and is fulfilled (fig. 11).

Therefore, we consider the subsample of events with $|\boldsymbol{p}_s| < 0.2$ GeV/$c$ as a sample of photon reactions on a target of quasi-free off-mass-shell neutrons. The calculation of cross sections in the spectator model proceeds as in ref. [7]. All cross sections are then raised by 22%, in order to correct for the restriction in the spectator momentum. This correction was determined from the fraction of events with $|\boldsymbol{p}_s| > 0.2$ GeV/$c$. Possible effects of the Pauli exclusion principle on the two final state protons, of multiple scattering and of shadowing cannot be calculated since the phase and spin dependence of the amplitude are not known. There are 4933 events assigned to reaction (7) after the acceptance cuts in t (see subsect. 2.3) and $|\boldsymbol{p}_s|$ are made. Among these events, 1788 have $E_\gamma^{\text{eff}} > 1.1$ GeV, i.e. are above the rho production threshold.

*3.3.2. Cross section for the reaction* $\gamma n \to \pi^0\pi^- p$. Fig. 12 shows the total cross section of the reaction (8) for $E_\gamma^{\text{eff}}$ between threshold and 5 GeV (black dots). Corrections for multiple $\pi^0$ events have been applied (see below). No cut in $t = (p_\gamma - p_{\pi\pi})^2$ is made. The background from events with unresolved pion/proton ambiguities (see subsect. 2.3) was estimated from the results of that part of our experiment which was done with a tagged photon beam [6] and the contribution of this background to the total cross section of reaction (8) has been subtracted. This

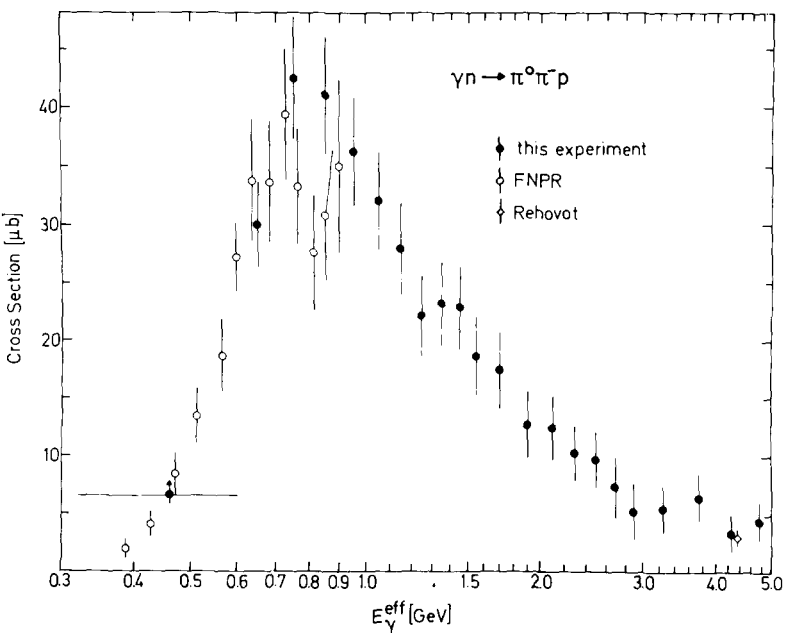


Fig. 12. Total cross section of the reaction $\gamma n \to \pi^0\pi^- p$ as a function of $E_\gamma^{\text{eff}}$. The black dots are our data, the open circles (diamonds) are taken from ref. [29] (ref. [4]).

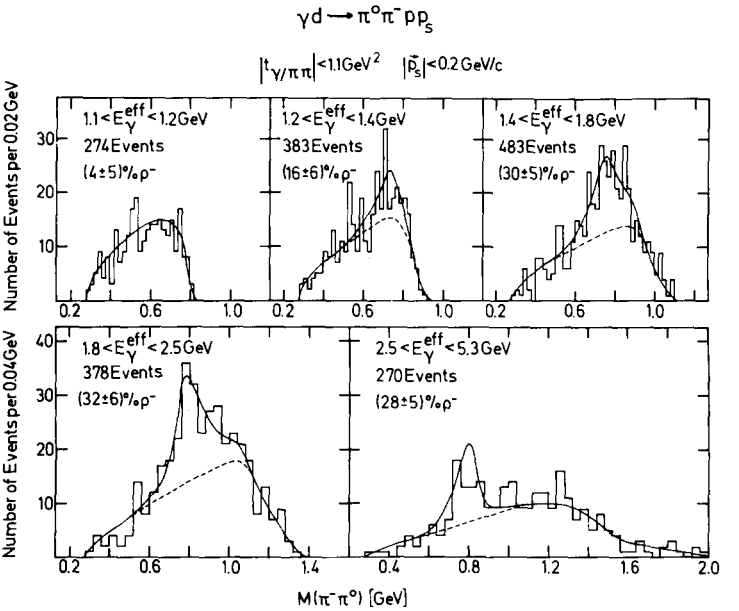


Fig. 13a.

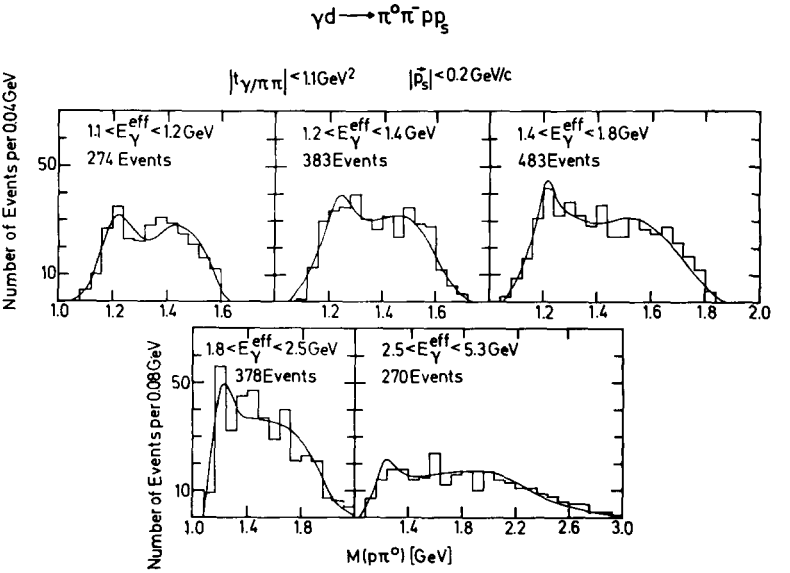


Fig. 13b.

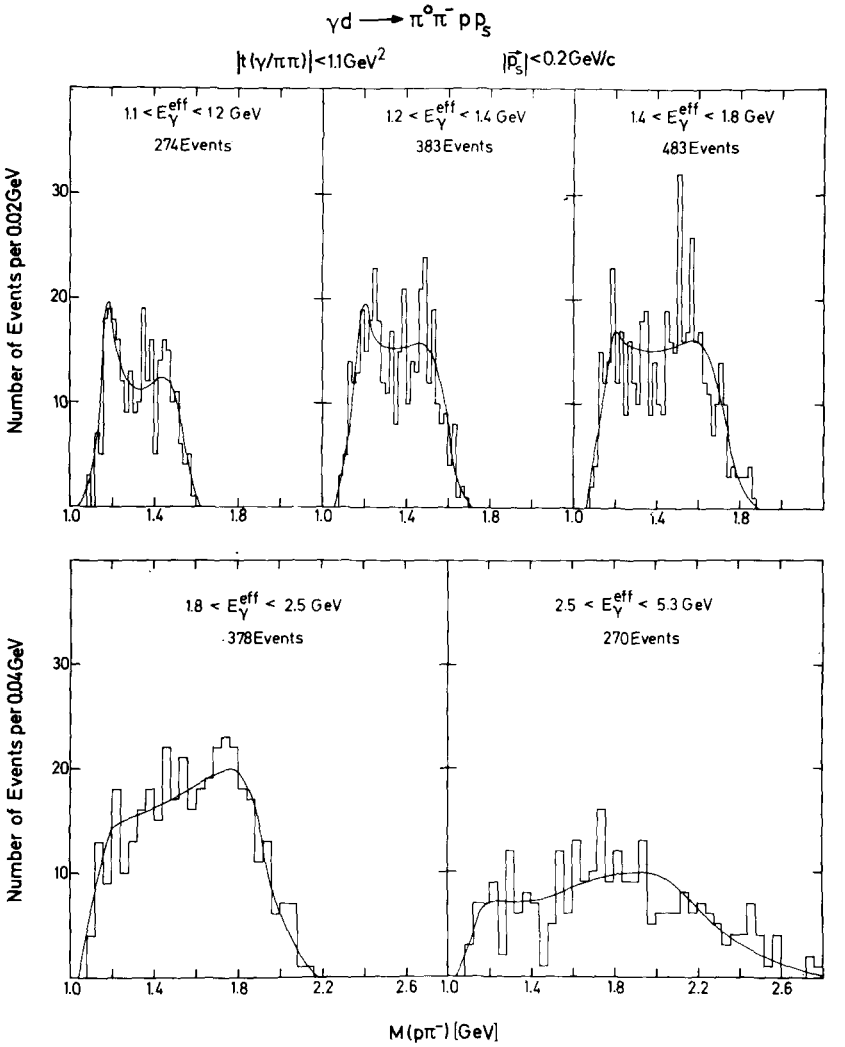


Fig. 13c.

Fig. 13. (a–c) Effective mass distributions of the $\pi^0\pi^-$, $\pi^0$p and $\pi^-$p systems in the reaction $\gamma n \to \pi^0\pi^- p$ (deduced from the reaction $\gamma d \to \pi^0\pi^- pp_s$) for $|t| < 1.1$ GeV$^2$ and various intervals of $E_\gamma^{\text{eff}}$. The curves are obtained from fits taking account of $\rho^-$, $\Delta^+$, $\Delta^0$ and phase space contributions.

correction is $\leqslant 10$ % for $E_\gamma^{\text{eff}} > 1.2$ GeV and negligible elsewhere. The results of the FNPR collaboration [29] (open circles) and the Weizmann group [4] (diamonds) are also shown in fig. 12. They are compatible with our data.

*3.3.3. $\rho^-$ production.* The effective mass distributions of the $\pi^0\pi^-$, $\pi^0$p and $\pi^-$p systems from reaction (8) are shown in figs. 13(a–c) for various intervals of $E_\gamma^{\text{eff}}$ between 1.1 and 5.3 GeV. The $t$-range is restricted to $|t| < 1.1$ GeV$^2$. Production of $\rho^-$, $\Delta^+(1236)$ and $\Delta^0$ (1236) is observed.

For a more detailed study of the reaction (3) we had to estimate the amount and distribution of the background from multiple $\pi^0$ production (see subsect. 2.3). This was done starting from "all charged" reactions like $\gamma n \to \pi^-\rho^0 p$ and $\gamma n \to \pi^-\pi^+\pi^-$p which can be completely separated from background. We assumed that the reactions $\gamma n \to \pi^0\rho^-$p and $\gamma n \to \pi^0\pi^0\pi^-$p, which contribute the bulk of the background to reactions (3) and (8), have similar mass distributions as the "all charged" reactions, and that their total cross sections can be estimated from the "all charged" reactions by assuming statistical weighting of the isospin states [30, 31]. We then studied how the photon energy $E_\gamma$ and the other calculated kinematical variables get changed if a single $\pi^0$ is substituted for the two $\pi^0$'s. In this way the background in the various

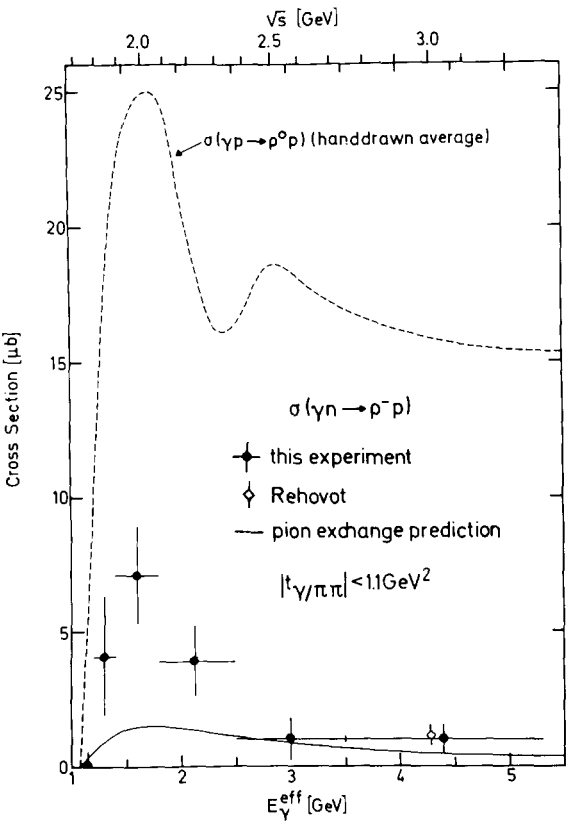


Fig. 14. Total cross section of the reaction $\gamma n \to \rho^-$p with the restriction $|t| < 1.1$ GeV$^2$ as a function of $E_\gamma^{\text{eff}}$ (black dots). Also shown is the result of the Weizmann group [4] (diamond). The full curve shows the pion exchange prediction for $\gamma n \to \rho^-$p, the dashed curve shows the qualitative energy behaviour of $\sigma(\gamma p \to \rho^0 p)$.

distributions was evaluated. It was found that depending on the kinematics part of the reaction $\gamma n \to \pi^0 \rho^- p$ is indistinguishable from the reaction $\gamma n \to \rho^- p$. This background ($\sim 0.5$ $\mu$b below and zero above 3.5 GeV) was therefore subtracted from our total $\rho^-$ cross sections. For differential cross sections the hypothesis of statistical mixing of the isospin states appears to be too uncertain to be applied directly; therefore our values of $d\sigma/dt$ ($\gamma n \to \rho^- p$) may be affected by some background from the reaction $\gamma n \to \pi^0 \rho^- p$.

The fraction of $\rho^-$ production was determined by fits assuming $\Delta^+$, $\Delta^0$ and $\rho^-$ production (using eq. (9)), as well as a phase-space background (curves in fig. 13). To take account of finite resolution effects and systematic shifts in the $\pi^0\pi^-$ mass distribution (see subsect. 2.3 and ref. [5]), the width of the $\rho^-$ was fixed at $\Gamma_{\rho^-} = 0.180$ GeV and its mass was taken as a free parameter.

*3.3.4. Total and differential cross sections for the reaction $\gamma n \to \rho^- p$.* The cross section $\sigma(\gamma n \to \rho^- p)$ for $|t| < 1.1$ GeV$^2$ obtained from these fits and corrected for multiple $\pi^0$ events is shown in fig. 14 as a function of $E_\gamma^{\text{eff}}$ (black dots). The cross section increases from threshold to a maximum value of about 7 $\mu$b at $E_\gamma^{\text{eff}} \approx 1.6$ GeV ($\sqrt{s} \approx 2$ GeV) and slowly decreases at higher energies. The result of the Weizmann group [4] (diamond) is also shown in fig. 14. It agrees with our data.

The differential cross sections $d\sigma/dt$ ($\gamma n \to \rho^- p$) were determined by repeating the fits indepently in various $t$ intervals. They are shown in fig. 15 for the $E_\gamma^{\text{eff}}$ range

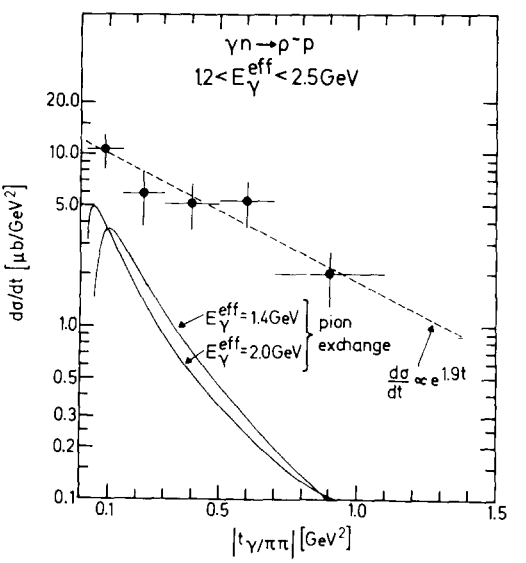


Fig. 15. Differential cross section for the reaction $\gamma n \to \rho^- p$ in the $E_\gamma^{\text{eff}}$ interval $1.2 < E_\gamma^{\text{eff}} < 2.5$ GeV. The first point at $t = 0.084$ GeV$^2$ is corrected for kinematic limits (see subsect. 3.3.4). The full curves show the pion exchange prediction. The dashed line shows an exponential with a slope of 1.9 GeV$^{-2}$.

1.2 to 2.5 GeV. The first point at $|t| = 0.084$ GeV$^2$ is corrected by +20 % for kinematic inaccessibilities due to the mass dependence of the minimum momentum transfer. The $t$-dependence of the differential cross section is weak. The dashed line shows an exponential with a slope of 1.9 GeV$^{-2}$.

## 4. Discussion of the results

### *4.1. Determination of the coupling constant ratio* $g^2_{\gamma\omega}/g^2_{\gamma\rho}$

In the framework of the vector-dominance model and of the additive quark model for elastic $\rho^0$ and $\omega$ scattering the cross -section ratio for $\omega$ and $\rho^0$ production on deuterons should be equal to the squared ratio of the $\gamma\omega$ and $\gamma\rho$ coupling constants. SU(3) with ideal $\omega\phi$ mixing gives the well-known result $g^2_{\gamma\omega} : g^2_{\gamma\rho} = 1 : 9$, but various symmetry-breaking schemes lead to slightly modified predictions: (0.65 : 9) [32] or (1.21 : 9) [33]. The $\rho^0$ cross section (obtained by assumption (i) on the resonance shape and corrected for the finite $\rho^0$ width, see subsect. 3.1) is $\sigma(\gamma d \to \rho^0 d) = 4.6 \pm 0.4$ $\mu$b for $1.4 < E_\gamma < 5.3$ GeV and $0.05 < |t| < 0.20$ GeV$^2$. Thus, with our result for $\sigma(\gamma d \to \omega d)$ (subsect. 3.2), we find

$$\frac{g^2_{\gamma\omega}}{g^2_{\gamma\rho}} = \frac{\sigma(\gamma d \to \omega d)}{\sigma(\gamma d \to \rho^0 d)} = 0.14 \begin{matrix} +0.03 \\ -0.07 \end{matrix} = (1.26 \begin{matrix} +0.30 \\ -0.62 \end{matrix}) : 9.$$

The experimental value for this ratio is less sensitive to scanning bias and normalization uncertainties than each cross section itself. The Weizmann group [4] found $g^2_{\gamma\omega}/g^2_{\gamma\rho} = 0.15 \pm 0.07$ from their $\rho^0$ and $\omega$ production data on deuterons at $E_\gamma$= 4.3 GeV. Both their and our values agree with the result $g^2_{\gamma\omega}/g^2_{\gamma\rho} = 0.14 \pm 0.02$ from $e^+e^-$ colliding beam experiments at Orsay [34].

### *4.2. Isospin analysis of the* $\rho^0$ *photoproduction amplitude*

*4.2.1. Comparison of* $\rho^0$ *production on protons and deuterons.* Starting from our measured data [35] on the reaction $\gamma p \to \rho^0 p$, we have calculated the expected differential cross section for coherent $\rho^0$ production on the deuteron (reaction (1)). In this calculation [3] we used the second order impulse approximation and also took the effects of the Fermi motion into account. Since our $\gamma d \to \rho^0 d$ data are at a rather small $|t|$, the dominating term in the amplitude is the single scattering term. In the limit that effects of the Fermi motion are relatively unimportant at our energies, the single scattering amplitude is proportional to the sum

$$T(\gamma p \to \rho^0 p) + T(\gamma n \to \rho^0 n) = 2T_0$$

of the $\rho^0$ production amplitudes on protons and neutrons, i.e. proportional to the $I = 0$ exchange amplitude $T_0$ on single nucleons, because the $I = 1$ exchange am-

plitude $T_1$ has different signs on protons and neutrons. Thus, the differential cross section $d\sigma/dt$ ($\gamma d \to \rho^0 d$) is essentially proportional to $|T_0|^2$ while the differential cross section for $\rho^0$ production on protons is proportional to $|T_0 + T_1|^2$.

In the calculation of the amplitude of reaction (1) we assumed $T_0$ to be helicity conserving and mainly imaginary, i.e. Re $T_0$/Im $T_0 = -0.20$ [36, 37]. The phase of $T_0$ enters in the interference between single and double scattering, but due to the smallness of the latter the dependence of the cross section on the phase is not at all critical. Double scattering in the deuteron causes a decrease of the cross section by about 9% in our $E_\gamma$ and $t$ region; the elastic $\rho^0$N scattering amplitudes that enter in the double scattering calculation were derived from the SLAC measurements in the double scattering region [2] which are consistent with the $\rho^0$ photoproduction data on complex nuclei and also with the quark and vector dominance models.

Since we do not know $|T_0|^2$, we made an approximate calculation of $d\sigma/dt$ ($\gamma d \to \rho^0 d$) in which we replaced $|T_0|^2$ by $|T_0 + T_1|^2$ as obtained from our measured data [35] on $d\sigma/dt$ ($\gamma p \to \rho^0 p$). By comparison with the measured $d\sigma/dt$ ($\gamma d \to \rho^0 d$) we thus obtain the ratio

$$R \equiv \frac{d\sigma/dt\,(\gamma d \to \rho^0 d)_{calc}}{d\sigma/dt\,(\gamma d \to \rho^0 d)_{meas}} \approx \frac{|T_0 + T_1|^2}{|T_0|^2} = 1 + \frac{|T_1|}{|T_0|}\, 2\cos\Delta\phi + \frac{|T_1|^2}{|T_0|^2}, \qquad (13)$$

where $\Delta\phi$ is the relative phase of $T_0$ and $T_1$. In fig. 5 the comparison between the calculated and the measured $d\sigma/dt$ ($\gamma d \to \rho^0 d$) is made, and good agreement is found throughout the $E_\gamma$ and $t$ range measured. The calculated cross sections integrated over $t$ and the corresponding values of $R$ are given in table 2 for the $t$-range $0.04 < |t| < 0.20$ GeV$^2$. The $R$ values are consistent with one within 10 %.

Not much is known about $\Delta\phi$, except that it can be shown [38] to lie outside the range $90° \pm \psi$ where $(90° + \psi)$ is the absolute phase angle of $T_0$. $\psi$ has been experimentally determined [36, 37] to be approximately 12° to 16°. Thus, $|\cos\Delta\phi| \gtrsim 0.2$. Unfortunately the paucity of the data precludes any conclusion on the size of $|T_1/T_0|$ if

Table 2
Total cross sections for $\gamma d \to \rho^0 d$ in the $t$-range $0.04 < |t| < 0.20$ GeV$^2$

| $E_\gamma$ (GeV) | $\sigma$ ($\mu$b) [a] observed | $\sigma$ ($\mu$b) [b] calculated | $R$ |
|---|---|---|---|
| 1.8 – 2.5 | 6.3 ± 0.8 | 6.0 | 0.95 ± 0.15 |
| 2.5 – 3.5 | 5.3 ± 0.7 | 5.7 | 1.08 ± 0.18 |
| 3.5 – 5.3 | 4.9 ± 0.7 | 5.4 | 1.10 ± 0.20 |
| 1.8 – 5.3 | 5.3 ± 0.5 | 5.6 | 1.06 ± 0.15 |

[a] Obtained with assumption (i) on the resonance shape (see subsect. 3.1.2).
[b] The calculated cross sections have uncertainties of about 10 % which come both from the errors of the input data and from approximations in the calculation.

$\cos \Delta\phi < 0$. On the other hand, if $\cos \Delta\phi > 0$, from eq. (13) and our values of R it follows that $|T_1/T_0| < 0.3$ within one standard deviation for the energy range $1.8 < E_\gamma < 5.3$ GeV. Further information on $|T_1/T_0|$ will be derived in the next section.

*4.2.2. Comparison of $\rho^-$ production on neutrons with $\rho^0$ production on protons.* The full curves in figs. 14 and 15 show the pion exchange (OPE) cross section [39] for $\rho^-$ production, using $\Gamma_{\rho\pi\gamma} = \frac{1}{9}\,\Gamma_{\omega\pi\gamma} = 0.13$ MeV as expected from SU(3) and the quark model. It is compatibel with the data for $E_\gamma^{\text{eff}} > 2.5$ GeV but fails at lower energies. The difference between the data and the OPE prediction may be partly due to $\rho^-$ exchange. Calculations of its contribution [40] are very sensitive to the value of the magnetic moment of the $\rho$ and are too uncertain up to now to draw further conclusions.

Also shown in fig. 14 is the qualitative behaviour of $\sigma(\gamma p \to \rho^0 p)$. For $E_\gamma^{\text{eff}} > 3$ GeV the $\rho^-$ cross section is less than $\frac{1}{10}$ of the $\rho^0$ cross section and even in the low-energy region $\rho^-$ production is not stronger than about $\frac{1}{3}$ of $\rho^0$ production, i.e. $I = 0$ exchange (P, P') obviously dominates in $\rho^0$ production also at low energies. The measurement of $\sigma(\gamma n \to \rho^- p)$ allows to further investigate the contribution of $I = 1$ exchange to $\rho^0$ production on nucleons. Principal exchanges are

$$\mathrm{P},\ \mathrm{P}',\ \pi^0,\ \mathrm{A}_2^0 \text{ for } \gamma p \to \rho^0 p,$$

$$\pi^-,\ \rho^-,\ \mathrm{A}_2^- \text{ for } \gamma n \to \rho^- p.$$

At high energies the exchange contributions of $\pi$ and $\rho$ or $\pi$ and $A_2$ do not interfere [41] and if one assumes that $\rho^-$ and $A_2^-$ exchange in $\rho^-$ production do not essentially cancel one can estimate the $I = 1$ exchange contribution by

$$\sigma(\gamma p \to \rho^0 p)^{(\pi^0 + \mathrm{A}_2^0)} \lesssim \tfrac{1}{2}\,\sigma(\gamma n \to \rho^- p)^{(\pi^- + \rho^- + \mathrm{A}_2^-)} = \tfrac{1}{2}\,(1.0 \pm 0.5)\,\mu\mathrm{b}$$

for $E_\gamma^{\text{eff}} > 3.5$ GeV. Thus for $\rho^0$ production one finds

$$\frac{\sigma(\gamma p \to \rho^0 p)^{(I=1 \text{ exchange})}}{\sigma(\gamma p \to \rho^0 p)^{\text{total}}} \lesssim 5\ \%$$

within one standard deviation, which however still allows 30 (20) % in amplitude for $\cos \Delta\phi > 0 (< 0)$, where $\Delta\phi$ is the relative phase of the $I = 0$ and $I = 1$ exchange amplitudes. This is consistent with the results from the previous section. It is also consistent with the small contribution from $\pi^0$ exchange found by the SBT collaboration [42] in $\rho^0$ production. At $E_\gamma = 4.7$ GeV they found $\sigma^{\mathrm{U}}(\gamma p \to \rho^0 p)/\sigma^{\text{tot}}(\gamma p \to \rho^0 p) = (-1.1 \pm 2.8)\%$, where $\sigma^{\mathrm{U}}$ is the unnatural parity exchange cross section.

*4.2.3. Isospin of the s-channel peaks in $\rho^0$ and $\rho^-$ photoproduction.* In the s-channel picture the peak of the $\rho^-$ cross section at $\sqrt{s} \approx 2$ GeV may be due to excitation of s-channel resonances via $\gamma n \to (N \text{ or } \Delta\ (\sim 2\ \text{GeV})) \to \rho^- p$. A rough estimate of their formation cross section from fig. 14 gives 6 $\mu$b (after subtraction of the OPE contribution), i.e. approximately half of that for $\rho^0$ production assuming a diffractive background of about 15 $\mu$b there. A ratio of $\sigma(\gamma n \to (N \text{ or } \Delta) \to \rho^- p)$: $\sigma(\gamma p \to (N \text{ or } \Delta) \to \rho^0 p) = 1 : 2$ favoures the dominance of $I = \frac{3}{2}$ resonances, whereas for the excitation of $I = \frac{1}{2}$ resonances the ratio would be 2 : 1. Possible candidates are the F35 (1890), P31 (1910) and F37 (1950). From the measured $\gamma N$ and $\rho N$ decay widths [43] of these $\Delta$ resonances, one expects their contributions to the reaction $\gamma n \to \Delta \to \rho^- p$ to be $\sim 1.8$ $\mu$b, $\sim 0.1$ $\mu$b and $\sim 1.7$ $\mu$b respectively at the resonance energies.

*4.3. Isospin exchange in $\omega$ photoproduction*

Since only $I = 0$ can be exchanged in the reaction $\gamma d \to \omega d$, neglecting multiple scattering corrections one has

$$\frac{d\sigma/dt\,(\gamma d \to \omega d)}{d\sigma^N/dt\,(\gamma p \to \omega p)} \approx \frac{4\,|T_0^N|^2}{|T_0^N + T_1^N|^2}\,, \tag{14}$$

where $T_0^N$ and $T_1^N$ are the natural parity, isospin 0 (P and P′) and 1 ($A_2$) exchange amplitudes, respectively, for $\gamma p \to \omega p$. The ratio between our $\gamma d \to \omega d$ cross section and the natural parity exchange part of $\gamma p \to \omega p$ from the SBT collaboration [44] is consistent with 4, i.e. with vanishing $A_2$ exchange. (A more precise estimation of the $A_2$ exchange in forward $\omega$ photoproduction on protons can be deduced in the vector-dominance model from the total $\gamma p$ and $\gamma n$ cross sections, using the relation [45]

$$\left.\frac{\operatorname{Im} T_1^N\,(\gamma p \to \omega p)}{\operatorname{Im} T_0^N\,(\gamma p \to \omega p)}\right|_{t=0} \approx \frac{1}{2}\left(\frac{g_{\gamma\rho}}{g_{\gamma\omega}}\right)^2 \frac{\sigma_{tot}\,(\gamma p) - \sigma_{tot}\,(\gamma n)}{\sigma_{tot}\,(\gamma p) + \sigma_{tot}\,(\gamma n)}\,; \tag{15}$$

measurements [46] give $0.110 \pm 0.025$ for the right-hand side between 2 and 4 GeV.)

*4.4. Test of duality and Regge factorization*

Roberts and Roy [47] have noted that semi-local Harari-Freund duality and factorization of Regge exchange provide a simple way to relate pion and photon induced reactions. For the pion exchange contributions to the reactions $\pi^- p \to \rho^0 n$ and $\gamma n \to \rho^- p$ one predicts

$$\frac{\sigma^{(\pi)}(\gamma n \to \rho^- p)}{\sigma^{(\pi)}(\pi^- p \to \rho^0 n)} = \frac{1}{2}\,\frac{\beta_{P'\gamma\gamma}}{\beta_{P'\pi\pi}}\,, \tag{16}$$

where $\beta_{P'\pi\pi}$ and $\beta_{P'\gamma\gamma}$ are the $\pi\pi$ and the $\gamma\gamma$ couplings of the leading trajectory P' in resonant $\pi\pi$ and $\gamma\pi$ scattering. The right-hand side of eq. (16) can be evaluated from Regge analysis of the total $\pi$N and $\gamma$N cross sections to be 0.0023. The reaction $\pi^- p \to \rho^0 n$ is expected to be dominated by pion exchange and its cross section at 4.3 GeV beam momentum is about 750 $\mu$b [48]. For the pion exchange contribution in $\gamma n \to \rho^- p$ we can give the upper limit $\sigma^{(\pi)}(\gamma n \to \rho^- p) \leqslant \sigma(\gamma n \to \rho^- p) = 1.0 \pm 0.5$ $\mu$b for $E_\gamma^{\text{eff}} > 3.5$ GeV, and thus the left-hand side of eq. (16) is

$$\frac{\sigma^{(\pi)}(\gamma n \to \rho^- p)}{\sigma^{(\pi)}(\pi^- p \to \rho^0 n)} \lesssim 0.0013 \pm 0.0007,$$

i.e. still barely compatible with the semi-local factorization prediction.

We thank M.W. Teucher and E. Lohrmann for their interest and encouragement, H. Meyer and H. Spitzer for their participation in the early stages of this experiment, and G. Horlitz and S. Wolff for an efficient run of the bubble chamber. This work was supported by the Bundesministerium für Forschung und Technologie.

## References

[1] G. McClellan et al., Phys. Rev. Letters 22 (1969) 374.
[2] R.L. Anderson et al., Phys. Rev. D4 (1971) 3245.
[3] H.G. Hilpert et al., Aachen-Bonn-Hamburg-Heidelberg-München Collaboration, Nucl. Phys. B23 (1970) 45.
[4] Y. Eisenberg et al., Nucl. Phys. B42 (1972) 349.
[5] H.G. Hilpert et al., Aachen-Bonn-Hamburg-Heidelberg-München Collaboration, Nucl. Phys. B21 (1970) 93.
[6] R. Schiffer et al., Aachen-Bonn-Hamburg-Heidelberg-München Collaboration, Nucl. Phys. B38 (1972) 628.
[7] P. Benz et al., Aachen-Bonn-Hamburg-Heidelberg-München Collaboration, Nucl. Phys. B65 (1973) 158.
[8] CERN program library, X-601, unpublished.
[9] D. Gall, Diplomarbeit, Hamburg 1971, unpublished.
[10] J. Ballam et al., Phys. Rev. Letters 24 (1970) 955.
[11] S.D. Drell, Phys. Rev. Letters 5 (1960) 278.
[12] P. Söding, Phys. Letters 19 (1966) 702.
[13] A.S. Krass, Phys. Rev. 159 (1967) 1496.
[14] V. Franco and R.J. Glauber, Phys. Rev. 142 (1966) 1195.
[15] J. Pumplin, Phys. Rev. D2 (1970) 1859.
[16] T. Bauer, Phys. Rev. Letters 25 (1970) 485.
[17] D.R. Yennie, Proc. of the 11th session of the Scottish Universities Summer School in Physics 1970, ed. J. Cummings and H. Osborn (1971), p. 321.
[18] F. Gutbrod, private communication.
[19] J.D. Jackson, Nuovo Cimento 34 (1964) 1644.
[20] C. Zemach, Phys. Rev. 133B (1964) 1201.

[21] M.S. Rabin et al., Phys. Rev. Letters 24 (1970) 925.
[22] D.G. Coyne et al., Nucl. Phys. B32 (1971) 333.
[23] U. Idschok, Thesis, Bonn Univ. PIB 3-21 (1972), unpublished.
[24] F. Storim, Thesis, internal report DESY F1-73/1 (1973), unpublished,
[25] T. Hamada and I.D. Johnston, Nucl. Phys. 34 (1962) 382.
[26] C. Michael and C. Wilkin, Nucl. Phys. B11 (1969) 99.
[27] S.B. Treiman and C.N. Yang, Phys. Rev. Letters 8 (1962) 140.
[28] L.I. Gutay et al., Phys. Letters 16 (1965) 343.
[29] A. Piazza et al., Nuovo Cimento Letters 3 (1970) 403.
[30] J. Shapiro, Nuovo Cimento Suppl. 18 (1960) 40.
[31] H. Satz, Phys. Letters 25B (1967) 27; Phys. Rev. Letters 19 (1967) 1453.
[32] R.J. Oakes and J.J. Sakurai, Phys. Rev. Letters 19 (1967) 1266.
[33] T. Das, V.S. Mathur and S. Okubo, Phys. Rev. Letters 19 (1967) 470.
[34] D. Benaksas et al., Phys. Letters 39B (1972) 289;
D. Benaksas et al., Phys. Letters 42B (1972) 507.
[35] Aachen-Berlin-Bonn-Hamburg-Heidelberg-München Collaboration, Phys. Rev. 175 (1968) 1669.
[36] H. Alvensleben et al., Phys. Rev. Letters 25 (1970) 1377.
[37] P.J. Biggs et al., Phys. Rev. Letters 27 (1971) 1157.
[38] D. Julius, Nucl. Phys. B33 (1971) 558.
[39] G. Wolf, SLAC-PUB-544 and private communication.
[40] N. Levy, M. Glück and S. Wagner, Phys. Rev. D4 (1971) 874.
[41] K. Schilling, P. Seyboth and G. Wolf, Nucl. Phys. B15 (1970) 397.
[42] J. Ballam et al., Phys. Rev. D5 (1972) 545.
[43] Particle Data Group, Review of particle properties, Rev. Mod. Phys. 45 (1973) no. 2, Part II.
[44] J. Ballam et al., Phys. Rev. D7 (1973) 3150.
[45] H. Harari, Proceedings of the 4th Int. Symp. on electron and photon interactions at high energies, Liverpool 1969, p. 107.
[46] T.A. Armstrong et al., Nucl. Phys. B41 (1972) 445.
[47] R.G. Roberts and D.P. Roy, Phys. Letters 47B (1973) 247.
[48] E. Bracci et al., CERN/HERA 72-1 (1972).